J. Fluid Mech. (1997), *vol.* 332, *pp.* 157–184

A systems theory approach to the feedback stabilization of infinitesimal and finite-amplitude disturbances in plane Poiseuille flow

By SANJAY S. JOSHI†, JASON L. SPEYER AND JOHN KIM

School of Engineering and Applied Science, University of California, Los Angeles
Los Angeles, CA 90024, USA

(Received 14 February 1995 and in revised form 15 July 1996)

A systems theory framework is presented for the linear stabilization of two-dimensional laminar plane Poiseuille flow. The governing linearized Navier–Stokes equations are converted to control-theoretic models using a numerical discretization scheme. Fluid system poles, which are closely related to Orr–Sommerfeld eigenvalues, and fluid system zeros are computed using the control-theoretic models. It is shown that the location of system zeros, in addition to the well-studied system eigenvalues, are important in linear stability control. The location of system zeros determines the effect of feedback control on both stable and unstable eigenvalues. In addition, system zeros can be used to determine sensor locations that lead to simple feedback control schemes. Feedback controllers are designed that make a new fluid–actuator–sensor–controller system linearly stable. Feedback control is shown to be robust to a wide range of Reynolds numbers. The systems theory concepts of modal controllability and observability are used to show that feedback control can lead to short periods of high-amplitude transients that are unseen at the output. These transients may invalidate the linear model, stimulate nonlinear effects, and/or form a path of 'bypass' transition in a controlled system. Numerical simulations are presented to validate the stabilization of both single-wavenumber and multiple-wavenumber instabilities. Finally, it is shown that a controller designed upon linear theory also has a strong stabilizing effect on two-dimensional finite-amplitude disturbances. As a result, secondary instabilities due to infinitesimal three-dimensional disturbances in the presence of a finite-amplitude two-dimensional disturbance cease to exist.

1. Introduction

A basic problem in fluid dynamics is the theoretical understanding of how instability in laminar shear flow leads to transition to turbulence. Since laminar flow is preferred in many applications, the suppression of fluid instabilities to maintain laminar flow would be very useful. Towards this goal, active boundary layer control of instability has been proposed. The nonlinear aspects of the transition process are still not clearly known. It has been shown (Orszag & Patera 1983) that some shear flows may sustain two-dimensional finite-amplitude instabilities that cause infinitesimal three-dimensional disturbances to be highly unstable. This two-dimensional primary instability/three-dimensional secondary instability process may be one nonlinear mechanism that leads to transition. Conversely, the behaviour of infinitesimal

† Present address: Jet Propulsion Laboratory, 4800 Oak Grove Drive, Pasadena, CA 91109, USA.

(linear) disturbances in laminar shear flow is well understood (Orr 1907; Sommerfeld 1908; Drazin & Reid 1981). Therefore, linear analysis provides a natural starting point to begin to develop active control schemes that may eventually lead to full transition control. It is the purpose of this paper to develop feedback controllers based on linear theory that stabilize two-dimensional plane Poiseuille flow to infinitesimal disturbances. In addition, it will be shown that a controller designed upon linear theory has a strong stabilizing effect on two-dimensional finite-amplitude instabilities. As a result, secondary three-dimensional instabilities as described in Orszag & Patera (1983) cease to exist in such a system.

Most prior work in the area of laminar flow linear instability suppression has concentrated on the wave superposition approach. A nice survey of past work is given in Joslin, Erlebacher & Hussaini (1994). The basic idea is that boundary layer instabilities appear as a combination of many sinusoidally growing waves of certain frequencies, phases, and amplitudes. If these wave parameters are known, or if they can be determined, a second wave may be stimulated in the flow that is exactly out of phase with the instability wave. In this way, the two waves may destructively interfere and flow may be stabilized. Disturbance of the flow field to cause a wave motion to appear has been experimentally demonstrated using several methods such as vibrating ribbons (Schubauer & Skramstad 1947), vibrating wires (Milling 1981), and heating elements (Nosenchuck 1982). In addition, several authors have numerically obtained wave superposition results based on Navier–Stokes simulations (Beringen 1984; Metcalfe *et al.* 1986). Most of the results, however, report incomplete destruction of instability waves. Joslin *et al.* (1994) explain that wave cancellation is very sensitive to the wave parameters and postulate that incomplete destruction reported in past studies was due to improper phase or amplitude properties of the cancelling wave.

In addition, Bower, Kegelman & Pal (1987) considered the Orr–Sommerfeld equation in designing an input to channel flow that may counteract the effects of a disturbance that excites instabilities. They showed that if an oscillating flat pulse function at the lower boundary of a channel excited inherent instabilities, a second oscillating flat pulse function could be constructed downstream that negated excitement of the instabilities. Much like the wave superposition approach, their aim was not to stabilize the underlying dynamics of the problem, but rather to 'cancel' the effects of a specific disturbance.

Unlike past work, our aim is to use systems theory to construct a combination fluid–actuator–sensor–controller *system* that is inherently stable. In essence, the approach changes the philosophy of the problem from thinking about how inputs can mitigate an inherently unstable system to thinking about how sensors and actuators can be added to form an entirely new *stable* system. Recently, mathematical control systems theory has begun to be applied to fluid systems (Burns & Ou 1994; Gunzburger, Hou & Suobodny 1992; Choi, Moin & Kim 1993). A control theory approach for laminar flow linear instability suppression will be shown to have several advantages over the traditional wave cancellation approach. It will eliminate the need to explicitly measure phase and frequency of instabilities. Also, it will provide a framework to select sensor locations in order to have the least complex controller. Further, feedback control will be shown to be extremely robust to changing Reynolds numbers given proper sensor location. In addition, linear feedback controllers will be shown to have a strong stabilizing effect on two-dimensional finite-amplitude disturbances.

This paper is organized as follows. In §2, we formulate the linear channel flow problem using the linearized Navier–Stokes equations. Boundary input in the form

of blowing/suction and boundary output in terms of shear are represented within the equations. In §3, we introduce the concepts of zeros and poles of a system, as well as control-theoretic models. The governing partial-differential equation for the system is converted into a set of first-order, ordinary differential equations via a Galerkin method. These first-order, ordinary differential equations are then converted into a control-theoretic model. Section 4 describes the infinite-dimensional nature of the channel flow system and how it affects the selection of actuation. Section 5 describes the numerical model and the verification of the calculated poles and zeros. Section 6 introduces feedback control design. It is shown that judicious sensor placement, based on zero locations, can lead to simple control schemes. Furthermore, the control system is extremely robust to change in Reynolds number. Section 7 explores unobservable modal reinforcement as a possible path of 'bypass' transition in a controlled system. It then shows how a particular control model, called the modal-canonical state space model, may be used to assess observability of modal reinforcement. Section 8 demonstrates multiple-wavenumber instability control. Section 9 demonstrates that a linear controller has a strong stabilizing effect on two-dimensional, finite-amplitude instabilities. As a result, secondary three-dimensional instabilities as described by Orszag & Patera (1983) cease to exist. Finally, §10 outlines conclusions.

2. Problem formulation

2.1. *Dynamic equations*

We consider two-dimensional plane Poiseuille flow between two parallel stationary plates. Let the channel be of finite length and finite height, with the centreline at zero. The flow in the channel is described by the unsteady nonlinear incompressible Navier–Stokes equations. In order to study the linear stability of the system, we follow the standard procedure. Consider small perturbations in the velocities of $\hat{u}(x, y, t)$ in the horizontal direction, $\hat{v}(x, y, t)$ in the vertical direction, and $\hat{p}(x, y, t)$ in the pressure field. Let the primary flow be represented by $U(y)$ with U_c being the centreline velocity. The linearized incompressible Navier–Stokes equations may be formed by substituting the primary flow and small perturbations into the nonlinear incompressible Navier–Stokes equations and disregarding the second-order terms involving the perturbations,

$$\frac{\partial \hat{u}(x,y,t)}{\partial t} + U(y)\frac{\partial \hat{u}(x,y,t)}{\partial x} + \frac{\mathrm{d}U(y)}{\mathrm{d}y}\hat{v}(x,y,t) = -\frac{\partial \hat{p}(x,y,t)}{\partial x} + \frac{1}{Re}\nabla^2\hat{u}(x,y,t), \tag{2.1}$$

$$\frac{\partial \hat{v}(x,y,t)}{\partial t} + U(y)\frac{\partial \hat{v}(x,y,t)}{\partial x} = -\frac{\partial \hat{p}(x,y,t)}{\partial y} + \frac{1}{Re}\nabla^2\hat{v}(x,y,t), \tag{2.2}$$

$$\frac{\partial \hat{u}(x,y,t)}{\partial x} + \frac{\partial \hat{v}(x,y,t)}{\partial y} = 0, \tag{2.3}$$

where the flow variables are non-dimensionalized by the channel half-height, H, and centreline velocity, U_c. Re is the Reynolds number defined as $(U_c H/\nu)$ where ν is the kinematic viscosity. By introducing a 'stream function', $\psi(x, y, t)$,

$$\hat{u}(x,y,t) \triangleq \frac{\partial \psi(x,y,t)}{\partial y} \tag{2.4}$$

and

$$\hat{v}(x,y,t) \triangleq -\frac{\partial \psi(x,y,t)}{\partial x}, \tag{2.5}$$

(2.1)–(2.3) may be combined into a single equation,

$$\frac{\partial}{\partial t}\frac{\partial^2\psi}{\partial x^2} + \frac{\partial}{\partial t}\frac{\partial^2\psi}{\partial y^2} = -U(y)\frac{\partial^3\psi}{\partial x^3} - U(y)\frac{\partial}{\partial x}\frac{\partial^2\psi}{\partial y^2} + \frac{\mathrm{d}^2U(y)}{\mathrm{d}y^2}\frac{\partial\psi}{\partial x} + \frac{1}{Re}\nabla^2(\nabla^2\psi). \quad (2.6)$$

Assume periodic boundary conditions in the streamwise (x) direction. For channel flow, with rigid plates at $y = -1$ and $y = 1$, the no-slip boundary conditions become

$$\psi(x, y = -1, t) = 0, \quad (2.7)$$

$$\frac{\partial\psi}{\partial y}(x, y = -1, t) = 0, \quad (2.8)$$

$$\psi(x, y = 1, t) = 0, \quad (2.9)$$

$$\frac{\partial\psi}{\partial y}(x, y = 1, t) = 0. \quad (2.10)$$

With an initial condition

$$\psi(x, y, t = 0) = g(x, y) \quad (2.11)$$

the boundary value problem is completely formed. Existence and uniqueness of solutions for the linearized Navier–Stokes equations have been studied in Ladyzhenskaya (1969), Kreiss & Lorenz (1989), and Temam (1984). Equations (2.6)–(2.11) represent the starting point for construction of a feedback control system. These equations neither include any control terms nor do they describe any sensing of flow field variables.

2.2. *Boundary input*

We consider the case of blowing/suction at the lower wall of the channel. The boundary conditions are now modified from before to include boundary input, represented as the *known* separable function $q(t)w(x)f(y)$,

$$\psi(x, y = -1, t) = q(t)w(x)f(y = -1), \quad (2.12)$$

$$\frac{\partial\psi}{\partial y}(x, y = -1, t) = q(t)w(x)\frac{\partial f(y = -1)}{\partial y} = 0, \quad (2.13)$$

$$\psi(x, y = 1, t) = 0, \quad (2.14)$$

$$\frac{\partial\psi}{\partial y}(x, y = 1, t) = q(t)w(x)\frac{\partial f(y = 1)}{\partial y} = 0. \quad (2.15)$$

Note that these conditions constrain the function $f(y)$ such that

$$f(y = -1) \neq 0, \quad (2.16)$$

$$\frac{\partial f(y = -1)}{\partial y} = 0, \quad (2.17)$$

$$f(y = 1) = 0, \quad (2.18)$$

$$\frac{\partial f(y = 1)}{\partial y} = 0. \quad (2.19)$$

Many functions may be equally appropriate. One such function is

$$f(y) = \tfrac{1}{2}y^4 + \tfrac{1}{4}y^3 - y^2 - \tfrac{3}{4}y + 1. \quad (2.20)$$

In order to relate boundary conditions on ψ to blowing/suction in the wall-normal direction, we use (2.5) to relate $\hat{v}(x, y, t)$ and $\psi(x, y, t)$. Then (2.12) becomes

$$\hat{v}(x, y = -1, t) = -q(t)\frac{\partial w(x)}{\partial x} f(y = -1). \tag{2.21}$$

Note that $\hat{v}(x, y, t)$ is related to the *derivative* of $w(x)$. The homogeneous equation (2.6) and the inhomogeneous boundary condition (2.12) can be converted into an inhomogeneous equation with homogeneous boundary conditions by introducing

$$\phi(x, y, t) \triangleq \psi(x, y, t) - q(t)f(y)w(x). \tag{2.22}$$

Then by substituting into (2.6), we obtain

$$\begin{aligned}
\frac{\partial}{\partial t}\frac{\partial^2 \phi}{\partial x^2} + \frac{\partial}{\partial t}\frac{\partial^2 \phi}{\partial y^2} &= -U(y)\frac{\partial^3 \phi}{\partial x^3} - U(y)\frac{\partial}{\partial x}\frac{\partial^2 \phi}{\partial y^2} + \frac{\mathrm{d}^2 U(y)}{\mathrm{d}y^2}\frac{\partial \phi}{\partial x} + \frac{1}{Re}\frac{\partial^4 \phi}{\partial x^4} + 2\frac{1}{Re}\frac{\partial^2}{\partial x^2}\frac{\partial^2 \phi}{\partial y^2} \\
&+ \frac{1}{Re}\frac{\partial^4 \phi}{\partial y^4} - \frac{\partial q(t)}{\partial t}\frac{\partial^2 w(x)}{\partial x^2} f(y) - \frac{\partial q(t)}{\partial t} w(x)\frac{\partial^2 f(y)}{\partial y^2} - q(t)\frac{\partial^3 w(x)}{\partial x^3} U(y) f(y) \\
&- q(t)\frac{\partial w(x)}{\partial x} U(y)\frac{\partial^2 f(y)}{\partial y^2} + q(t)\frac{\partial w(x)}{\partial x}\frac{\mathrm{d}^2 U(y)}{\mathrm{d}y^2} f(y) + \frac{1}{Re} q(t)\frac{\partial^4 w(x)}{\partial x^4} f(y) \\
&+ 2\frac{1}{Re} q(t)\frac{\partial^2 w(x)}{\partial x^2}\frac{\partial^2 f(y)}{\partial y^2} + \frac{1}{Re} q(t) w(x)\frac{\partial^4 f(y)}{\partial y^4}.
\end{aligned} \tag{2.23}$$

The boundary conditions in terms of ϕ are now

$$\phi(y = -1) = 0, \tag{2.24}$$

$$\frac{\partial \phi(y = -1)}{\partial y} = 0, \tag{2.25}$$

$$\phi(y = 1) = 0, \tag{2.26}$$

$$\frac{\partial \phi(y = 1)}{\partial y} = 0. \tag{2.27}$$

2.3. *Boundary output*

We use the streamwise component of shear at a single boundary point, $z(x_i, y = -1, t)$, as our boundary output, which is given by

$$z(x_i, y = -1, t) = \frac{\partial \hat{u}(x_i, y = -1, t)}{\partial y}. \tag{2.28}$$

By expressing $\hat{u}(x_i, y = -1, t)$ in terms of the stream function (2.4),

$$z(x_i, y = -1, t) = \frac{\partial^2 \psi(x_i, y = -1, t)}{\partial y^2}, \tag{2.29}$$

and by observing (2.22)

$$z(x_i, y = -1, t) = \frac{\partial^2 \psi(x_i, y = -1, t)}{\partial y^2} = \frac{\partial^2 \phi(x_i, y = -1, t)}{\partial y^2} + q(t)\frac{\partial^2 f(y = -1)}{\partial y^2} w(x_i). \tag{2.30}$$

3. Zeros, eigenvalues, and control-theoretic models

Linear stability analysis of (2.6) (Drazin & Reid 1981) shows that the system is linearly unstable for a range of Reynolds numbers. The goal of this paper is to

stabilize the system using control theory. To do this, we first transform the governing equations into special control-theoretic models.

3.1. *System transfer function*

We have defined a single-input/single-output (SISO) system in the sense that only one scalar function, $q(t)$, defines the entire input and one scalar function, $z(t)$, defines the output. A common form of control model for a finite-dimensional SISO system is the transfer function model. The transfer function, $H(s)$, is defined as the Laplace transform of the output, $z(t)$, divided by the Laplace transform of the input, $q(t)$, where zero initial conditions are assumed. Then

$$H(s) \triangleq \frac{\mathscr{L}[z(t)]}{\mathscr{L}[q(t)]} = \frac{Z(s)}{Q(s)}. \tag{3.1}$$

For finite-dimensional systems, $Z(s)$ and $Q(s)$ take the form of polynomials in the complex variable s. These polynomials may be factored to yield an equivalent representation,

$$H(s) \triangleq \frac{Z(s)}{Q(s)} = \frac{\prod_{j=1}^{J}(s-\zeta_j)}{\prod_{i=1}^{I}(s-p_i)}. \tag{3.2}$$

In this form, $p_1 \ldots p_I$ are the *poles* of the system. The poles of any system are dependent solely on the physics of the underlying system, independent of any particular input or output. Unstable modes of the system appear as poles whose real part is greater than zero. As will be seen in later sections, the poles are closely related to the eigenvalues of the Orr–Sommerfeld equation. The values $\zeta_1 \ldots \zeta_J$ are the *zeros* of the system. They are heavily dependent on which particular inputs and outputs are used on the system. As will be seen later, the position of these zeros will dictate sensor locations and will reveal the effect of feedback control on the eigenvalues. A graphical representation of the transfer function can be produced by plotting the poles and zeros in the complex s-space.

3.2. *State-variable model*

Much of modern control theory is based on the state-variable representation of a dynamic system. This representation relies on the basic fact that the motion of any finite-dimensional dynamic system may be expressed as a set of first-order ordinary differential equations. As a simple example of a state variable model (Franklin, Powell & Emami-Naeini 1988), Newton's law for a constant single mass, M, moving in one dimension, x, under a force, $F(t)$, is

$$M\frac{\mathrm{d}^2x(t)}{\mathrm{d}t^2} = F(t). \tag{3.3}$$

If we define one state variable as the position $x_1 \triangleq x(t)$ and the other state variable as the velocity $x_2 \triangleq \mathrm{d}x(t)/\mathrm{d}t$, (3.3) can be written as

$$\frac{\mathrm{d}x_1}{\mathrm{d}t} = x_2, \tag{3.4}$$

$$\frac{\mathrm{d}x_2}{\mathrm{d}t} = \frac{F(t)}{M}. \tag{3.5}$$

Furthermore, the first-order linear ordinary differential equations can be expressed using matrix notation

$$\begin{bmatrix} \dfrac{\mathrm{d}x_1}{\mathrm{d}t} \\ \dfrac{\mathrm{d}x_2}{\mathrm{d}t} \end{bmatrix} = \begin{bmatrix} 0 & 1 \\ 0 & 0 \end{bmatrix} \begin{bmatrix} x_1 \\ x_2 \end{bmatrix} + \begin{bmatrix} 0 \\ 1 \end{bmatrix} \frac{F}{M} \tag{3.6}$$

or

$$\frac{\mathrm{d}\boldsymbol{x}}{dt} = \boldsymbol{A}\boldsymbol{x} + \boldsymbol{B}q. \tag{3.7}$$

If we take output as position, x_1,

$$z = \begin{bmatrix} 1 & 0 \end{bmatrix} \begin{bmatrix} x_1 \\ x_2 \end{bmatrix} \tag{3.8}$$

or

$$z = \boldsymbol{C} \cdot \boldsymbol{x} \tag{3.9}$$

The matrix $\boldsymbol{A}$, and the vectors $\boldsymbol{B}$ and $\boldsymbol{C}$ are called the state space matrices of the single-input, single-output (SISO) system. More specifically, the $\boldsymbol{A}$ matrix is referred to as the dynamic matrix of the system. It can be shown that the poles of the system are simply the eigenvalues of the $\boldsymbol{A}$ matrix. In the more general case of multiple-input, multiple-output (MIMO) systems, $\boldsymbol{B}$ and $\boldsymbol{C}$ are matrices. For generality, we may add another term, $\boldsymbol{D}q$, to the output equation to account for systems in which there is direct feedthrough from the input to the output. Then,

$$z = C \cdot \boldsymbol{x} + Dq \tag{3.10}$$

In the case of no direct feedthrough, $D = 0$, the state space and transfer function models are related as

$$H(s) \triangleq \frac{Z(s)}{Q(s)} = \boldsymbol{C}(s\boldsymbol{I} - \boldsymbol{A})^{-1}\boldsymbol{B}. \tag{3.11}$$

3.3. *State-space formulation for channel system*

We will convert our problem into a set of first-order ordinary differential equations and then form a state-space model from these equations. The state-space model can then be represented with transfer function poles and zeros. We will proceed in this way for two reasons. First, our system lends itself to decomposition into first-order ordinary-differential equations by use of a Galerkin method. More importantly, however, the state-space model lends itself to extremely elegant ways to control eigenvalues of a system in well prescribed ways. It should be noted that unlike the single-mass example given above, the channel system requires an infinite number of ordinary differential equations to describe its motion. This is known as an infinite-dimensional system. As a result, any finite number of ordinary-differential equations used in a state-space model will not completely describe the system. The difficulties associated with such a system are taken up after a discussion of the Galerkin method used to obtain the ordinary-differential equations.

3.3.1. *First-order system*

We use a standard Galerkin procedure to convert the governing partial differential equation (2.23) into a system of ordinary-differential equations. Assume an

approximate solution of (2.23) as

$$\phi_a(x,y,t) \triangleq \sum_{n=-N}^{N}\sum_{m=0}^{M} a_{nm}(t)P_n(x)\Gamma_m(y). \tag{3.12}$$

By using Fourier functions, $e^{in\alpha_0 x}$, for $P_n(x)$ and basis functions constructed from Chebyshev polynomials for $\Gamma_m(y)$ (Joshi 1996), we obtain a first-order system. Define inner products in the streamwise (x) and normal (y) directions respectively:

$$[e^{in\alpha_0 x}, e^{im\alpha_0 x}]_x \triangleq \frac{1}{L}\int_{-L/2}^{L/2} e^{in\alpha_0 x}e^{-im\alpha_0 x}dx = \delta_{mn}, \qquad \alpha_0 \triangleq \frac{2\pi}{L}, \tag{3.13}$$

and

$$[\Gamma_m(y), \Gamma_n(y)]_y \triangleq \int_{-1}^{1} \frac{\Gamma_n(y)\Gamma_m(y)}{(1-y^2)^{1/2}}dy, \tag{3.14}$$

where L is the non-dimensional length of the finite-length channel. Applying the orthogonality of the basis functions in x, we obtain a system of first-order ordinary differential equations:

$$\begin{aligned}
&-\sum_{m=0}^{M}\frac{\partial a_{lm}(t)}{\partial t}l^2\alpha_0^2\beta_{mk}^0 + \sum_{m=0}^{M}\frac{\partial a_{lm}(t)}{\partial t}\beta_{mk}^2 = \sum_{m=0}^{M}a_{lm}(t)il^3\alpha_0^3\beta_{mk}^{0+} - \sum_{m=0}^{M}a_{lm}(t)il\alpha_0\beta_{mk}^{2+}\\
&+\sum_{m=0}^{M}a_{lm}(t)il\alpha_0\beta_{mk}^{0-} + \frac{1}{Re}\sum_{m=0}^{M}a_{lm}(t)l^4\alpha_0^4\beta_{mk}^0 - 2\frac{1}{Re}\sum_{m=0}^{M}a_{lm}(t)l^2\alpha_0^2\beta_{mk}^2\\
&+\frac{1}{Re}\sum_{m=0}^{M}a_{lm}(t)\beta_{mk}^4 + \frac{\partial q(t)}{\partial t}\{S_{lk}^1\} + q(t)\{S_{lk}^2\}, l = -N\ldots N, k = 0\ldots M,
\end{aligned} \tag{3.15}$$

where

$$S_{lk}^1 \triangleq -\left[\frac{\partial^2 w(x)}{\partial x^2}, P_l(x)\right]_x \left[v(y), \Gamma_k(y)\right]_y - \left[w(x), P_l(x)\right]_x \left[\frac{\partial^2 v(y)}{\partial y^2}, \Gamma_k(y)\right]_y \tag{3.16}$$

and

$$\begin{aligned}
S_{lk}^2 \triangleq &-\left[\frac{\partial^3 w(x)}{\partial x^3}, P_l(x)\right]_x [U(y)v(y), \Gamma_k(y)]_y - \left[\frac{\partial w(x)}{\partial x}, P_l(x)\right]_x \left[U(y)\frac{\partial^2 v(y)}{\partial y^2}, \Gamma_k(y)\right]_y\\
&+\left[\frac{\partial w(x)}{\partial x}, P_l(x)\right]_x \left[\frac{d^2U(y)}{dy^2}v(y), \Gamma_k(y)\right]_y + \frac{1}{Re}\left[\frac{\partial^4 w(x)}{\partial x^4}, P_l(x)\right]_x [v(y), \Gamma_k(y)]_y\\
&+2\frac{1}{Re}\left[\frac{\partial^2 w(x)}{\partial x^2}, P_l(x)\right]_x \left[\frac{\partial^2 v(y)}{\partial y^2}, \Gamma_k(y)\right]_y + \frac{1}{Re}[w(x), P_l(x)]_x \left[\frac{\partial^4 v(y)}{\partial y^4}, \Gamma_k(y)\right]_y.
\end{aligned} \tag{3.17}$$

In this system, α_0 is the fundamental wavenumber in the x-direction, defined as $2\pi/L$, and the β coefficients are defined in terms of the following scalar products, where the $\Gamma(y)$ are the basis functions in y:

$$\beta_{mk}^j \triangleq \left[\frac{\partial^j \Gamma_m(y)}{\partial y^j}, \Gamma_k(y)\right]_y, \qquad j = 0\ldots 4, \tag{3.18}$$

$$\beta_{mk}^{0+} \triangleq [U(y)\Gamma_m(y), \Gamma_k(y)]_y, \tag{3.19}$$

$$\beta_{mk}^{0-} \triangleq \left[\frac{d^2U(y)}{dy^2}\Gamma_m(y), \Gamma_k(y)\right]_y, \tag{3.20}$$

$$\beta_{mk}^{2+} \triangleq \left[U(y) \frac{\partial^2 \Gamma_m(y)}{\partial y^2}, \Gamma_k(y) \right]_y . \tag{3.21}$$

3.3.2. *Transformation to state-space form*

We may visualize (3.15) in block matrix form as

$$\begin{bmatrix} M_{-N} & 0 & \cdots & 0 \\ 0 & M_{-N+1} & 0 & 0 \\ 0 & 0 & \ddots & 0 \\ 0 & 0 & 0 & M_N \end{bmatrix} \begin{bmatrix} \dfrac{\mathrm{d}\vec{a}_{l=-N}}{\mathrm{d}t} \\ \dfrac{\mathrm{d}\vec{a}_{l=-N+1}}{\mathrm{d}t} \\ \vdots \\ \dfrac{\mathrm{d}\vec{a}_{l=N}}{\mathrm{d}t} \end{bmatrix}$$

$$= \begin{bmatrix} K_{-N} & 0 & \cdots & 0 \\ 0 & K_{-N+1} & 0 & 0 \\ 0 & 0 & \ddots & 0 \\ 0 & 0 & 0 & K_N \end{bmatrix} \begin{bmatrix} \vec{a}_{l=-N} \\ \vec{a}_{l=-N+1} \\ \vdots \\ \vec{a}_{l=N} \end{bmatrix} + \begin{bmatrix} \Upsilon_1 & \Upsilon_2 \end{bmatrix} \begin{bmatrix} q(t) \\ \dfrac{\mathrm{d}q(t)}{\mathrm{d}t} \end{bmatrix} \tag{3.22}$$

where $\vec{a}_{l=p}$ denotes a column vector of all a_{lk} coefficients whose first index, l, is the value p. In compact notation,

$$\boldsymbol{M} \frac{\mathrm{d}\boldsymbol{a}}{\mathrm{d}t} = \boldsymbol{K}\boldsymbol{a} + \begin{bmatrix} \Upsilon_1 & \Upsilon_2 \end{bmatrix} \begin{bmatrix} q(t) \\ \dfrac{\mathrm{d}q(t)}{\mathrm{d}t} \end{bmatrix} . \tag{3.23}$$

Assuming non-singularity of the $\boldsymbol{M}$ matrix, we may invert to obtain

$$\frac{\mathrm{d}\boldsymbol{a}}{\mathrm{d}t} = \boldsymbol{M}^{-1}\boldsymbol{K}\boldsymbol{a} + \begin{bmatrix} \boldsymbol{M}^{-1}\Upsilon_1 & \boldsymbol{M}^{-1}\Upsilon_2 \end{bmatrix} \begin{bmatrix} q(t) \\ \dfrac{\mathrm{d}q(t)}{\mathrm{d}t} \end{bmatrix} \tag{3.24}$$

where $\boldsymbol{a}$, $\boldsymbol{K}$, Υ_1 and Υ_2 are all complex. By expanding in terms of real and imaginary parts, we obtain

$$\begin{aligned} \frac{\mathrm{d}\boldsymbol{a}_R}{\mathrm{d}t} + \mathrm{i}\frac{\mathrm{d}\boldsymbol{a}_I}{\mathrm{d}t} = {} & \boldsymbol{M}^{-1}\boldsymbol{K}_R\boldsymbol{a}_R + \mathrm{i}\boldsymbol{M}^{-1}\boldsymbol{K}_I\boldsymbol{a}_R + \mathrm{i}\boldsymbol{M}^{-1}\boldsymbol{K}_R\boldsymbol{a}_I - \boldsymbol{M}^{-1}\boldsymbol{K}_I\boldsymbol{a}_I \\ & + \boldsymbol{M}^{-1}\Upsilon_{1R}q(t) + \mathrm{i}\boldsymbol{M}^{-1}\Upsilon_{1I}q(t) + \boldsymbol{M}^{-1}\Upsilon_{2R}\frac{\mathrm{d}q(t)}{\mathrm{d}t} + \mathrm{i}\boldsymbol{M}^{-1}\Upsilon_{2I}\frac{\mathrm{d}q(t)}{\mathrm{d}t}. \end{aligned} \tag{3.25}$$

where the subscript R or I indicates real or imaginary parts. Define

$$\tilde{\boldsymbol{p}} \triangleq \begin{bmatrix} \boldsymbol{a}_R \\ \boldsymbol{a}_I \\ q(t) \end{bmatrix} . \tag{3.26}$$

Then the state space system is

$$\frac{\mathrm{d}\tilde{\boldsymbol{p}}}{\mathrm{d}t} = \begin{bmatrix} \boldsymbol{M}^{-1}\boldsymbol{K}_R & -\boldsymbol{M}^{-1}\boldsymbol{K}_I & \boldsymbol{M}^{-1}\Upsilon_{1R} \\ \boldsymbol{M}^{-1}\boldsymbol{K}_I & \boldsymbol{M}^{-1}\boldsymbol{K}_R & \boldsymbol{M}^{-1}\Upsilon_{1I} \\ 0 & 0 & 0 \end{bmatrix} \tilde{\boldsymbol{p}} + \begin{bmatrix} \boldsymbol{M}^{-1}\Upsilon_{2R} \\ \boldsymbol{M}^{-1}\Upsilon_{2I} \\ 1 \end{bmatrix} \frac{\mathrm{d}q(t)}{\mathrm{d}t} \tag{3.27}$$

We write (3.27) as

$$\frac{\mathrm{d}\tilde{\boldsymbol{p}}}{\mathrm{d}t} = \boldsymbol{A}\tilde{\boldsymbol{p}} + \boldsymbol{B}\frac{\mathrm{d}q(t)}{\mathrm{d}t} \triangleq \boldsymbol{A}\tilde{\boldsymbol{p}} + \boldsymbol{B}u(t) \tag{3.28}$$

where the input to the system is $\mathrm{d}q(t)/\mathrm{d}t$. Note since $q(t)$ in (2.12) is related to physical blowing/suction, it is important to keep in mind that the input to this model is the *derivative* of $q(t)$. In physical terms, any input derived from this model will be in terms of $\mathrm{d}q(t)/\mathrm{d}t$ and therefore must be integrated before it can be applied as physical blowing/suction.

3.3.3. *Measurement equations*

By observing (2.30) and using the assumed solution form (3.12)

$$z(x_i, y=-1, t) = \frac{\partial^2 \psi(x_i, y=-1, t)}{\partial y^2} = \frac{\partial^2 \phi}{\partial y^2} + q(t)\frac{\partial^2 f(y=-1)}{\partial y^2} w(x_i)$$
$$= \sum_{n=-N}^{N} \sum_{m=0}^{M} a_{nm}(t) P_n(x_i) \frac{\partial^2 \Gamma_m(y=-1)}{\partial y^2} + q(t)\frac{\partial^2 f(y=-1)}{\partial y^2} w(x_i) + \rho(t, x_i, y=-1) \tag{3.29}$$

where $\rho(t, x_i, y=-1)$, the residual component of streamwise shear due to the truncated expansion, is assumed to be negligible compared to the two other terms. The second term on the right-hand side of (3.29) is made up of the known input terms (2.12). Denote

$$D \triangleq \frac{\partial^2 f(y=-1)}{\partial y^2} w(x_i). \tag{3.30}$$

By pulling out the complex time coefficients and denoting them as the vector $\boldsymbol{a}$ as above we may construct a complex observation matrix, $\boldsymbol{O}$

$$z(x_i, y=-1, t) = \boldsymbol{O}\boldsymbol{a} + Dq(t). \tag{3.31}$$

Finally, by creating $\tilde{\boldsymbol{p}}$ by stacking the real and imaginary parts of $\boldsymbol{a}$, as well as $q(t)$, we may construct an observation equation in state-variable form

$$\begin{bmatrix} z_R(x_i, y=-1, t) \\ z_I(x_i, y=-1, t) \end{bmatrix} = \begin{bmatrix} \boldsymbol{O}_R & -\boldsymbol{O}_I & D \\ \boldsymbol{O}_I & \boldsymbol{O}_R & 0 \end{bmatrix} \tilde{\boldsymbol{p}}. \tag{3.32}$$

Since we may measure only real output (shear), we are left with only the top half of the observation matrix,

$$z_R(x_i, y=-1, t) = \begin{bmatrix} \boldsymbol{O}_R & -\boldsymbol{O}_I & D \end{bmatrix} \tilde{\boldsymbol{p}}. \tag{3.33}$$

In order to describe the system in traditional control terms, define

$$\boldsymbol{C} \triangleq \begin{bmatrix} \boldsymbol{O}_R & -\boldsymbol{O}_I & D \end{bmatrix}. \tag{3.34}$$

Then,

$$z_R(x_i, y=-1, t) = \boldsymbol{C}\tilde{\boldsymbol{p}} \tag{3.35}$$

3.3.4. *Initial conditions*

We have not accounted for the initial value (2.11) in our boundary value problem. We may account for the initial condition by assuming it can be written as a series expansion in terms of $P_n(x)$ and $\Gamma_m(y)$. Then

$$\phi(x, y, t=0) = \psi(x, y, t=0) - s(t=0)f(y)w(x) = g(x, y) - s(t=0)f(y)w(x)$$
$$= \sum_{n=-N}^{N} \sum_{m=0}^{M} b_{nm} P_n(x) \Gamma_m(y) \tag{3.36}$$

where b_{nm} are assumed known. Then

$$\boldsymbol{a}(t=0) = \boldsymbol{b}. \tag{3.37}$$

Since $\boldsymbol{a}$ and $\boldsymbol{b}$ are both complex, stack the real and imaginary components to arrive at an initial condition on $\tilde{\boldsymbol{p}}$:

$$\tilde{\boldsymbol{p}}(t=0) = \begin{bmatrix} \boldsymbol{b}_R \\ \boldsymbol{b}_I \\ q(t=0) \end{bmatrix}. \tag{3.38}$$

We have now defined the system completely in the state-variable form of (3.7), (3.9) where $\boldsymbol{A}$ and $\boldsymbol{B}$ are given in (3.28), $\boldsymbol{C}$ is given in (3.35), and the initial condition is (3.38). Although we have shown the state-space formulation using a single input and a single output, we may formulate the multiple input/multiple output case similarly. In that case, the multiple input functions are represented as a *sum* of separable functions in (2.12) and multiple outputs are represented as a vector whose components are of the form (3.35). It should be noted that in the multiple input case, it is important for physical implementation that for any finite stretch in the x-direction, only one of the multiple input functions is non-zero.

4. Infinite-dimensional nature of the channel problem and effect on actuator design

In a system described by partial–differential equations, such as the channel flow problem, no finite-dimensional model will capture all the dynamics of the system. Such a system is called infinite-dimensional. By examining the Galerkin approximate solution (3.12), we see that the approximate solution can converge only as $N, M \to \infty$. This would result in an infinite number of ordinary differential equations. Each n value included in the approximate solution is referred to as adding an additional wavenumber in the dynamic model. Even for just one wavenumber, $n = N$ (say), we see the assumed Galerkin solution requires an infinite number of terms in the y-direction,

$$\phi_a(x, y, t) \triangleq \sum_{m=0}^{M\to\infty} a_{Nm}(t) P_N(x) \Gamma_m(y). \tag{4.1}$$

Interestingly, by examining the structure of the $\boldsymbol{A}$ matrix in the resulting state-space model, we see that the dynamics associated with each individual wavenumber are decoupled from the others. This is characterized by a block diagonal form of the $\boldsymbol{A}$ matrix, (4.2). As a result, we may separate the problem of determining system poles into a set of smaller problems that include only one wavenumber at a time:

$$\boldsymbol{A} = \begin{bmatrix} [\boldsymbol{A}_{(n=1)}] & 0 & \cdots & \infty \\ 0 & [\boldsymbol{A}_{(n=2)}] & 0 & 0 \\ 0 & 0 & \ddots & 0 \\ \infty & 0 & 0 & [\boldsymbol{A}_{(n=\infty)}] \end{bmatrix}. \tag{4.2}$$

Indeed, the eigenvalues (poles) of the entire $\boldsymbol{A}$ matrix are simply the eigenvalues (poles) of each smaller $\boldsymbol{A}$ matrix block. Offsetting this computational advantage, however, is the fact that the locations of the zeros are not decoupled by wavenumber. Therefore, even though the poles of the system can be calculated separately using only one wavenumber in a particular computation, the zeros of the system force all

the wavenumbers in the model to be considered together. This can easily be seen from an examination of the transfer functions associated with just two wavenumbers. Consider two transfer functions obtained by using two distinct wavenumbers and the same input, $u(t)$, and output, $z(t)$:

$$H_{(n=1)} = \frac{N_{(n=1)}(s)}{D_{(n=1)}(s)}, \qquad H_{(n=2)} = \frac{N_{(n=2)}(s)}{D_{(n=2)}(s)}. \tag{4.3}$$

The roots of $N(s)$ are the zeros and the roots of $D(s)$ are the poles. In terms of input and output,

$$z = H_{(n=1)}u, \qquad z = H_{(n=2)}u. \tag{4.4}$$

Considered together, however,

$$z = \left[H_{(n=1)} + H_{(n=2)}\right] u = \left[\frac{D_{(n=2)}(s)N_{(n=1)}(s) + D_{(n=1)}(s)N_{(n=2)}(s)}{D_{(n=1)}(s)D_{(n=2)}(s)}\right] u. \tag{4.5}$$

The poles of the new, combined transfer function are clearly those of each model separately. The zeros, however, are the roots of a completely new polynomial $D_{(n=2)}(s)N_{(n=1)}(s) + D_{(n=1)}(s)N_{(n=2)}(s)$, which, in general, has little to do with either of the original numerators.

We have seen that an infinite expansion is needed to fully model the channel system. Since in practice an infinite expansion cannot be used to create a state-space model, we will always have some part of the system dynamics that is unmodelled. Furthermore, we have seen that the $\boldsymbol{A}$ (dynamic) matrix may be decoupled by wavenumber.

Consider a partition of the state-space model as

$$\frac{\mathrm{d}x}{\mathrm{d}t} = \begin{bmatrix} \dfrac{\mathrm{d}x_m}{\mathrm{d}t} \\ \dfrac{\mathrm{d}x_u}{\mathrm{d}t} \end{bmatrix} = \begin{bmatrix} \boldsymbol{A}_m & 0 \\ 0 & \boldsymbol{A}_u \end{bmatrix} \begin{bmatrix} x_m \\ x_u \end{bmatrix} + \begin{bmatrix} \boldsymbol{B}_m \\ \boldsymbol{B}_u \end{bmatrix} u(t), \tag{4.6}$$

$$z = \begin{bmatrix} \boldsymbol{C}_m & \boldsymbol{C}_u \end{bmatrix} x, \tag{4.7}$$

where the subscripts m and u represent the modelled and unmodelled parts of the system. In the channel flow problem, the unmodelled part is meant to denote only the dynamics of wavenumbers left out of the finite-dimensional model. Note that both $\boldsymbol{A}_u$ and $\boldsymbol{A}_m$ are of infinite dimension; $\boldsymbol{A}_u$ because of the infinite number of wavenumbers left out of the reduced-order model and $\boldsymbol{A}_m$ because of the infinite number of expansion functions needed in y for each of the finite number of modelled wavenumbers. One way to avoid considering unmodelled wavenumber dynamics is to ensure that the control input, $u(t)$, has no effect whatsoever on the unmodelled wavenumber dynamics. In terms of the state-space model (4.6), this is equivalent to rendering $\boldsymbol{B}_u = 0$. This is known as making the unmodelled wavenumber dynamics uncontrollable. By examining (3.27), we see that the $\boldsymbol{B}$ matrix is formed from terms of S^1_{lk} in (3.16). If $w(x)$ in (3.16) is such that $S^1_{lk} = 0$, then those components of the $\boldsymbol{B}$ matrix are zero. Equivalently, we must ensure that the projection of $w(x)$ onto the *unmodelled* wavenumbers is zero. Owing to the orthogonality of Fourier components, we select $w(x)$ to be made up of modelled Fourier components only.

5. Single-wavenumber channel model

Consider the channel model shown in figure 1. The total non-dimensional length of the channel, L, is 4π. In this case, the fundamental wavenumber, $\alpha_0 = 0.5$. Only one

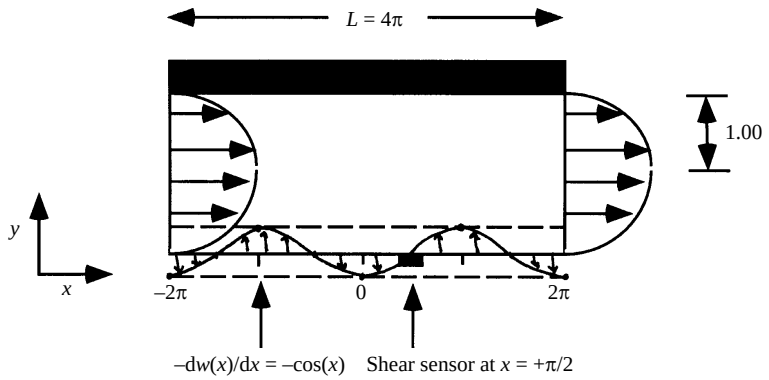

FIGURE 1. System model for Poiseuille flow. Input is applied along the bottom plate as $w(x) = \sin(x)$ and shear is measured at $x = \pi/2$ with $Re = 10\,000$ and $\alpha = 1.0$.

wavenumber is included in the model, corresponding to $\alpha = l\alpha_0 = 1.00$. The Reynolds number is chosen as $Re = 10\,000$. Input is distributed along the bottom plate with a sinusoidal weighting function in order to render the unmodelled wavenumber dynamics uncontrollable as described in §4. In terms of the input function, $w(x)$, see (2.12)

$$w(x) = \sin(x). \tag{5.1}$$

Note that the physical blowing/suction, $\hat{v}(x, y, t)$, takes the form

$$\hat{v}(x, y, t) = -q(t)\frac{\partial w(x)}{\partial x} f(y = -1) = -q(t)\cos(x) f(y = -1) \tag{5.2}$$

see (2.21). This type of input may be achieved in practice by a large number of independently controllable actuators that are distributed along the lower channel wall. The $f(y)$ function is chosen as in (2.20). The sensor location is $x = +\frac{1}{2}\pi$. In order to visualize the control-theoretic model, the system $\boldsymbol{A}$, $\boldsymbol{B}$, and $\boldsymbol{C}$ matrices are transformed to transfer function form, $H(s)$. Figure 2 shows the locations of the poles and zeros in the s-plane for the single-wavenumber model.

5.1. *Relation of poles to eigenvalues of the Orr–Sommerfeld equation*

Poles of the transfer function or, equivalently, eigenvalues of the $\boldsymbol{A}$ matrix are closely related to the eigenvalues of the Orr–Sommerfeld equation. Assume a solution of (2.6) of the form

$$\psi(x, y, t) \triangleq \beta(y) e^{i\alpha x} e^{-i\alpha c t}. \tag{5.3}$$

By substituting into (2.6), we obtain the familiar Orr-Sommerfeld equation in the normal-mode form,

$$[U(y) - c]\left(\frac{\partial^2 \beta(y)}{\partial y^2} - \alpha^2 \beta(y)\right) - \frac{\partial^2 U(y)}{\partial y^2}\beta(y) = \frac{1}{i\alpha Re}\left[\frac{\partial^4 \beta(y)}{\partial y^4} - 2\alpha^2 \frac{\partial^2 \beta(y)}{\partial y^2} + \alpha^4 \beta(y)\right]. \tag{5.4}$$

Here, the Reynolds number, Re, is known; the wavenumber, α, is assumed real and known; the complex wave speed, c, is the eigenvalue of the problem; and the function $\beta(y)$ is the eigenvector of the problem. Stability of a flow for a given value of Re and α is determined by the imaginary part of c. If the imaginary part is positive, the solution (5.3) becomes an unbounded exponential and flow is unstable. Poles of the

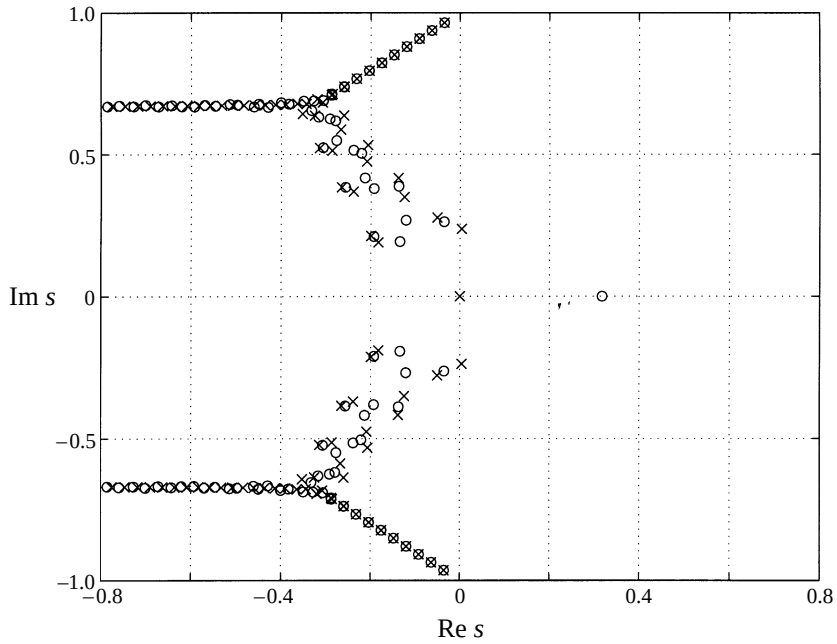

FIGURE 2. Pole (×) and zero (o) configuration for the system model of figure 1. Note that all poles and zeros appear in complex-conjugate pairs. Each pair of complex-conjugate poles represents one mode of the system. One pair of poles is to the right of the imaginary axis. This indicates the system has one unstable mode. Note that the single pole at the origin represents a built-in integrator due to $u(t) = \mathrm{d}q(t)/\mathrm{d}t$. Channel model: $Re = 10\,000$, shear sensor at $\pi/2$,$w(x) = \sin(x)$, $L = 4\pi$, $\alpha = 1.0$.

transfer function in the Laplace domain at $s = p_i$ correspond to solutions in the time domain of $\mathrm{e}^{p_i t}$. As a result, we observe that poles of the transfer function are related to eigenvalues of the Orr–Sommerfeld equation as

$$p_i \equiv -\mathrm{i}\alpha c. \tag{5.5}$$

In order to validate our linear code, we compare our poles to eigenvalues produced in Orszag (1971). Orszag (1971) obtained Orr-Sommerfeld eigenvalues for the channel problem with $\alpha = 1.00$ and $Re = 10\,000$. He reported only one slightly unstable eigenvalue at $s = 0.00373967 + \mathrm{i}0.23752649$ ($c = 0.23752649 - \mathrm{i}0.00373967$). The eigenvalue is seen as unstable by its positive real part. We obtained identical results including the one unstable mode at

$$s = 0.00373967 \mp \mathrm{i}0.23752649.$$

All other stable modes obtained in the present study are identical to those reported in Orszag (1971). The goal of our control system will be to move these unstable poles into the stable half of the s-plane or, equivalently, make sure the controlled-system poles all have real parts less than zero.

5.2. *Verification of model zeros*

Verification of the system zeros is more difficult due to the fact that no published results exist to our knowledge. We use the channel code simulation used in Kim, Moin & Moser (1987) to verify our zeros. This code is a spectral channel flow code which uses periodic boundary conditions. Consider the transfer function model (3.2)

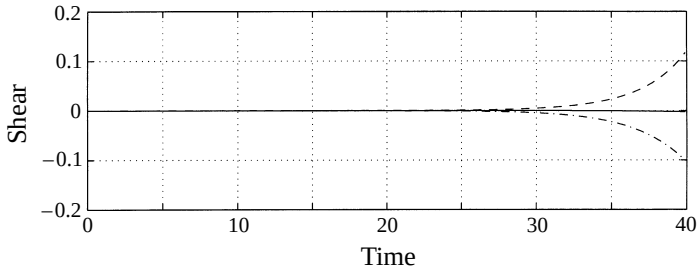

FIGURE 3. Output from the Navier–Stokes simulation with input applied as $u(t) = e^{+0.317557t}$. Although an unbounded input is applied, near zero output is observed at sensor location $\pi/2$ (solid curve). Sensor location 0 (dashed curve) and sensor location π (dash-dot curve) do not show zero output. Channel model: $Re = 10\,000$, shear sensor at $\pi/2$,$w(x) = \sin(x)$, $L = 4\pi$, $\alpha = 1.0$.

with $J = 1$ and $I = 1$:

$$H(s) = \frac{Z(s)}{U(s)} = \frac{(s - \zeta_1)}{(s - p_1)}. \tag{5.6}$$

In the Laplace domain,

$$sZ(s) - p_1 Z(s) = sU(s) - \zeta_1 U(s). \tag{5.7}$$

Assuming zero initial conditions and transforming into the time domain, (5.7) becomes

$$\frac{dz(t)}{dt} - p_1 z(t) = \frac{du(t)}{dt} - \zeta_1 u(t) \tag{5.8}$$

where $z(t)$ is the output function and $u(t)$ is the input function. If the input is taken as

$$u(t) = e^{\zeta_1 t} \tag{5.9}$$

then the right-hand side of (5.8) becomes zero and the system behaves as if zero input has been applied. As a result, $z(t)$ remains zero for all time. Therefore, we may verify zeros of the system by applying non-zero input in special ways and observing zero output. Note from figure 2 that for sensor location $x = +\frac{1}{2}\pi$, one zero exists in the right half plane at $s = +0.317557 + 0\mathrm{i}$. This represents an ideal zero to check as this corresponds to an unbounded, unstable input. Figure 3 shows output from the Navier–Stokes simulation with input $u(t) = dq(t)/dt = e^{+0.317557t}$. Note that even though an unbounded, exponentially growing input is applied to the system, near zero output is observed at the sensor, thus verifying that ζ_1 is indeed a zero of the system. This is contrasted with measurements at different sensor locations that grow rapidly. With a sensor at a different location, the zeros of the system change position so zero output is no longer expected for this particular input. Absolute zero is not observed at sensor location $x = \frac{1}{2}\pi$ due to slight numerical inaccuracies in the model.

6. Feedback control and stabilization

At this point, with the construction of a valid state-variable model, any number of control schemes may be employed to stabilize the system. A general control system is shown in figure 4. The output of the system is fed into a controller. The output of the controller is then used to create an input to the system. The design of a controller that achieves certain system characteristics is the goal of control system design. Several

modern control techniques may be applied that require a state-variable model. In this paper, the primary goal will be system stability. For this purpose, a simple constant gain feedback with integral compensator will be shown to be sufficient.

6.1. *Constant gain feedback with integral compensator*

Figure 5 shows an integral compensator feedback control scheme. K is referred to as the gain of the feedback. The output of the system, in this case shear, is multiplied by a feedback gain, integrated in time, and then fed back as blowing and suction at the input. Note that the integrator is required because of the structure of the input given in (3.27), i.e. the input is taken as the derivative of suction/blowing. The signal, $r(t)$, is called the reference signal. It is used to define the desired output. In our case, we would like the shear output, $z(x_i, y = -1, t)$, to be zero. Therefore, we set $r(t)$ to zero. Then

$$u(t) \triangleq \frac{\partial q(t)}{\partial t} = -K z(x_i, y = -1, t). \tag{6.1}$$

Therefore, assuming $q(0) = 0$,

$$q(t) = -K \int_0^t z(x_i, y = -1, \tau) \mathrm{d}\tau \tag{6.2}$$

and by observing (2.21), we may describe physical blowing and suction at the boundary:

$$\hat{v}(x, y = -1, t) = -q(t) \frac{\partial w(x)}{\partial x} f(y = -1) = K \cos(x) \int_0^t z(x_i, y = -1, \tau) \mathrm{d}\tau \tag{6.3}$$

As defined earlier,

$$H(s) \triangleq \frac{\mathscr{L}[z(t)]}{\mathscr{L}[u(t)]} = \frac{Z(s)}{U(s)}. \tag{6.4}$$

Therefore,

$$Z(s) = H(s) U(s). \tag{6.5}$$

In the absence of feedback, one mode is unstable. Also, one pole exists at the origin for the integrator. Consider a new transfer function from the reference input, $r(t)$, to the output, $z(t)$, in the presence of feedback:

$$u(t) = r(t) - K z(t). \tag{6.6}$$

By taking the Laplace transform of (6.6),

$$U(s) = R(s) - K Z(s). \tag{6.7}$$

Then

$$Z(s) = H(s)[R(s) - K Z(s)]. \tag{6.8}$$

Finally,

$$\frac{Z(s)}{R(s)} = \frac{H(s)}{1 - K H(s)}. \tag{6.9}$$

The new poles of the feedback system are defined by

$$1 - K H(s) = 0. \tag{6.10}$$

As K gets larger and larger, it is clear that the poles of the new system tend toward the zeros of $H(s)$. In this way, modes of the system can sometimes be changed to

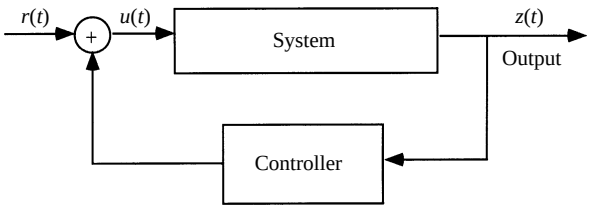

FIGURE 4. Feedback control. The output of the system is fed into a controller and then to the input.

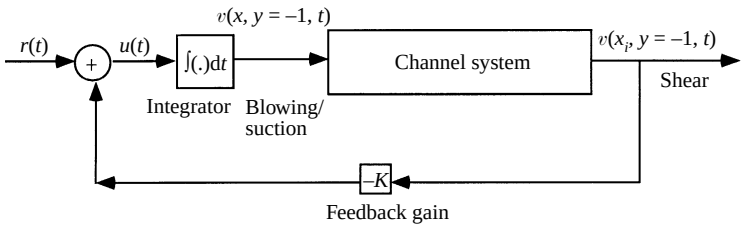

FIGURE 5. Feedback control for channel system. The output of the system is multiplied by a feedback gain, integrated in time, and then fed back at the input. The reference signal, $r(t)$, equals 0.

form a stable system (Franklin *et al.* 1988). Unstable modes that appear as poles on the right hand side of the complex s-plane and 'marginally stable' poles on the Im(s)-axis are drawn to the left-hand side by applying feedback.

6.2. *Sensor placement*

We have seen that, by applying feedback, poles of the system will eventually be drawn to zeros of the system. In the channel flow system of figure 2, any feedback will cause either the pole at the origin (integrator pole) or the unstable mode poles to be drawn to the zero on the real axis in the right-hand plane, thus making the system unstable to a greater degree. Therefore, finding a transfer function that has all zeros in the left-hand plane becomes an important objective. The poles of the system are independent of sensing or actuation. However, the zeros of the system are dependent on both the type and location of sensing and the type and location of actuation. Figure 6 shows the pole/zero configuration for the channel model with the shear sensor at three different locations. Only the top half of the s-plane is shown since the bottom half is a mirror image projected across the real axis as shown in figure 2. The poles of all the models are in the same location as expected. However, the zeros are different in all three cases. In figures 6(a) and 6(b), we observe a lone zero in the right-hand s-plane. However, when the sensor is placed at $x = +\pi$, figure 6(c) shows all zeros in the left-hand plane. In fact, there is a region around $x = \pi$ that results in all zeros in the left-hand plane. By placing a shear sensor at $x = \pi$, simple feedback with integral compensation will allow stabilization with the proper value of gain, K. In the case of sensor locations that result in right-hand-plane, so called 'non-minimum phase', zeros stabilization is still possible. However, more complex controllers (Bryson & Ho 1975; Ogata 1990) must be designed that are beyond the scope of this paper.

6.3. *Root locus analysis and numerical simulation*

One way to visualize how system poles will change as the feedback gain, K, changes is to construct a root locus plot. This is a plot of all poles of a system as the feedback

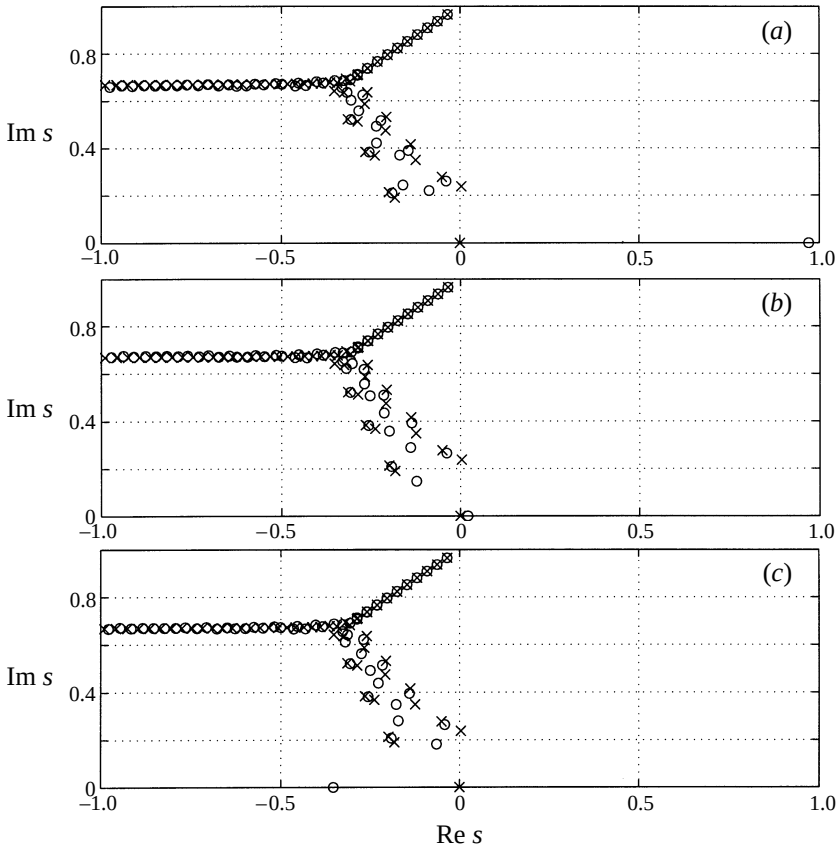

FIGURE 6. Pole (×)/zero (o) configuration. Channel model: $Re = 10\,000$, $w(x) = \sin(x)$, $L = 4\pi$, $\alpha = 1.0$. Only the top half of the s-plane is shown. Shear sensor at (a) $\pi/4$ (b) $3\pi/4$, (c) π.

gain varies from $K = 0$ to $K = \infty$. Figure 7 shows such a plot for the system shown in figure 6(c). When K reaches 0.1, all feedback system poles (closed-loop-poles) lie on the left-hand plane and no instabilities exist in the new feedback system. Numerical results obtained from the Navier–Stokes simulation for the new feedback controlled system are shown in figure 8. The computation is carried out without feedback until $t = 50$, after which the feedback is turned on. We see that the growing instability is quickly suppressed. At the instant the controller is turned on, the simulation shows a high transient response due to the non-continuous nature of the input at that time instant. In terms of the state space defined in (3.28), (3.35),

$$\frac{\mathrm{d}\tilde{\boldsymbol{p}}}{\mathrm{d}t} = \boldsymbol{A}\tilde{\boldsymbol{p}} + \boldsymbol{B}u(t), \tag{6.11}$$

$$z(x_i, y = -1, t) = C\tilde{\boldsymbol{p}}, \tag{6.12}$$

$$u(t) = -\boldsymbol{K}z(x_i, y = -1, t). \tag{6.13}$$

Then, in a closed loop,

$$\frac{\mathrm{d}\tilde{\boldsymbol{p}}}{\mathrm{d}t} = \boldsymbol{A}\tilde{\boldsymbol{p}} - \boldsymbol{B}(\boldsymbol{K}z(x_i, y = -1, t)) \tag{6.14}$$

$$= \boldsymbol{A}\tilde{\boldsymbol{p}} - \boldsymbol{B}\boldsymbol{K}\boldsymbol{C}\tilde{\boldsymbol{p}} = (\boldsymbol{A} - \boldsymbol{B}\boldsymbol{K}\boldsymbol{C})\tilde{\boldsymbol{p}} \tag{6.15}$$

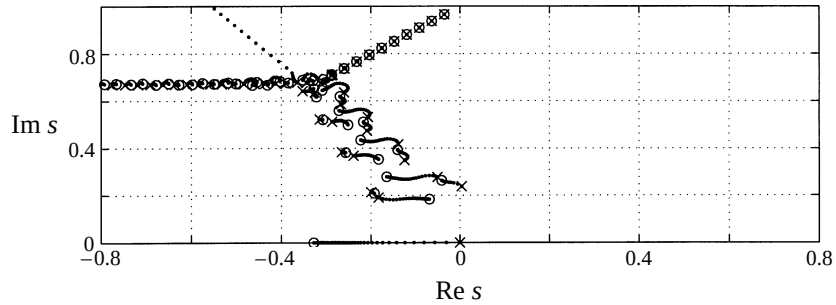

FIGURE 7. Root locus plot for channel system with input as in the channel model (figure 1) and shear output at $x = \pi$. The poles start at the open-loop poles shown with $\times$'s. As K increases, they start to move toward the location of the system zeros, shown as o's. The pole at position $s = (0,0)$ moves directly to the left. The unstable pole moves quickly to a position just to the left of the imaginary axis. Near $0.7 < y < 1.0$, $-0.6 < x < -0.4$, we see a pole moving towards a zero that is out of the range of this figure. Channel model: $Re = 10\,000$, shear sensor at π, $w(x) = \sin(x)$, $L = 4\pi$, $\alpha = 1.0$. Only the top half of the s-plane is shown.

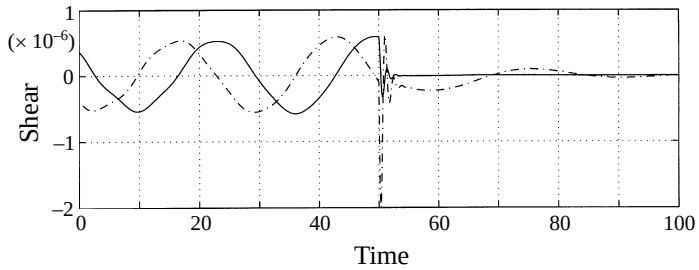

FIGURE 8. Navier–Stokes simulation of feedback control. Shear is multiplied by a feedback gain, integrated, and fed back into the input. Channel model: $Re = 10\,000$, feedback shear sensor at π, $w(x) = \sin(x)$, $L = 4\pi$, $\alpha = 1.0$. Curve 1 (solid) shows shear at location π; curve 2 (dot-dash) shows shear at location $\pi/2$.

The solution to this equation is

$$\tilde{\boldsymbol{p}}(t) = \mathrm{e}^{\boldsymbol{A}t - \boldsymbol{BKC}t}\tilde{\boldsymbol{p}}(t = 0). \tag{6.16}$$

This solution will approach zero as $t \to \infty$ since the eigenvalues of $\boldsymbol{A} - \boldsymbol{BKC}$ (closed-loop poles) are all stable.

6.4. *Robustness in the presence of Reynolds number uncertainty*

A major advantage of feedback control systems is their robustness to system uncertainty. From a practical point of view, Reynolds numbers may not be known exactly or may change frequently as in the flight of an airplane, for example. Figure 9 shows the open-loop pole/zero configurations for systems with varying Reynolds numbers. Note that these systems start with all zeros in the left-hand s-plane. A root locus analysis shows that a feedback system with $K = 0.1$ stabilizes both systems. Indeed, a feedback gain of $K = 0.1$ stabilizes systems for a wide range of Reynolds numbers from $Re = 1000$ to $Re = 40\,000$. Figure 10 shows the least-stable pole in both the controlled and uncontrolled systems for several Reynolds numbers. Recall that a pole with real part less than zero is stable. We see near $Re = 5772$, an unstable pole appears in the open-loop (uncontrolled) system. Unstable eigenvalues continue to exist in the open-loop system until

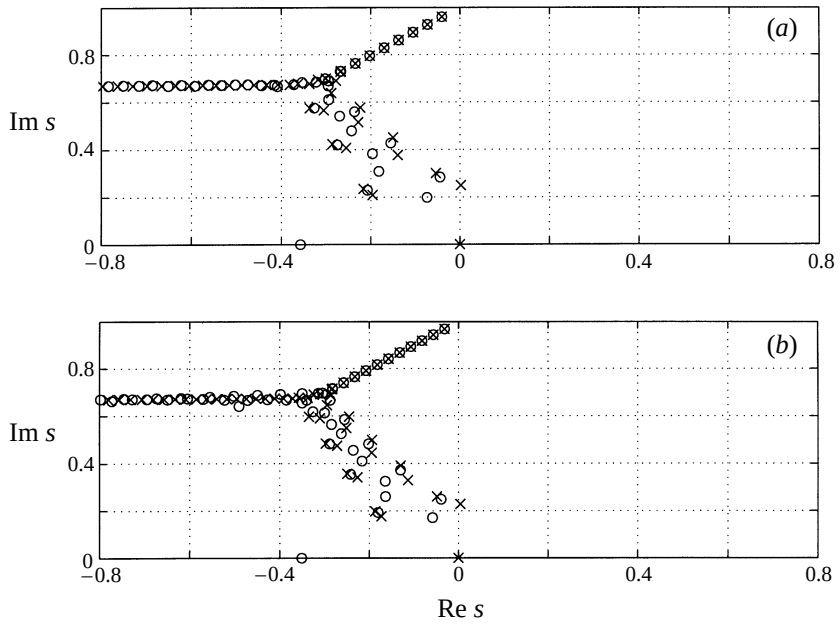

FIGURE 9. Pole (×)/zero (o) configuration. Channel model: shear sensor at π, $w(x) = \sin(x)$, $L = 4\pi$, $\alpha = 1.0$. Only the top half of the s-plane is shown. (a) $Re = 7500$, (b) $Re = 12\,500$.

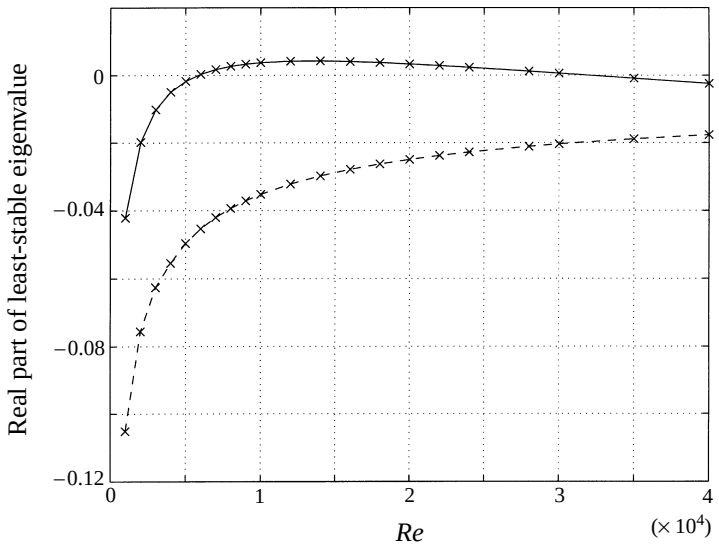

FIGURE 10. Real part of least-stable pole for open-loop (solid line) and closed-loop (dashed line) channel system with $1000 \leqslant Re \leqslant 40\,000$. Shear sensor at π, $w(x) = \sin(x)$, $L = 4\pi$, $\alpha = 1.0$. Data points are shown as ×'s.

$30\,000 \leqslant Re \leqslant 35\,000$. An identical feedback controller, with gain $K = 0.1$, however, stabilizes the system for Reynolds numbers in the range $1000 \leqslant Re \leqslant 40\,000$. Clearly, the feedback controller is extremely robust to changes in Reynolds number.

7. Unobservable transient response as a path of bypass transition

Recently, some authors (Trefethen *et al.* 1993; Butler & Farrell 1992; Farrell 1988; Henningson 1994) have suggested a possible path of bypass transition in Poiseuille flow that is caused by high transient response due to the non-self-adjointness of the evolution matrix. This high-transient behaviour is due to the non-orthogonality of the eigenmodes and not caused by any single mode, but rather a combination of many modes. In this section, we suggest a possible different form of bypass transition *in a controlled system* due to a single mode. In the presence of any type of control, it is possible that energy from an input is fed into a mode such that the mode is reinforced during the transient period before it eventually dies out. During the transient period, however, the mode may grow to an amplitude large enough to trigger nonlinear effects that induce transition to turbulence. This may be a possible path of bypass transition in a controlled system.

Single modes may be characterized in linear systems in terms of modal controllability and modal observability. Modal controllability implies that a particular mode may be affected by the actuators chosen (blowing/suction in our case). Modal observability implies that a particular mode may be measured by the sensors chosen (shear in our case). A particular mode may be non-observable, non-controllable, or both. This will be seen in §§7.1 and 7.2. If high-transient modes are controllable and observable, control theory may be used to suppress them. However, if high-transient modes are unobservable, the high transients will never be seen and feedback control cannot be used to suppress them.

7.1. *Modal canonical form*

The state-space formulation provides an excellent framework for assessing the reinforcement of each mode individually. Consider an n-dimensional state space with scalar input and output

$$\frac{\mathrm{d}\boldsymbol{x}}{\mathrm{d}t} = \boldsymbol{A}\boldsymbol{x} + \boldsymbol{B}u, \tag{7.1}$$

$$z = \boldsymbol{C}\boldsymbol{x}. \tag{7.2}$$

We may perform a similarity transformation on the system to produce a new state-space representation with the same input–output relationship, but with a different interpretation of the state variables. Let

$$\boldsymbol{P} \triangleq \begin{bmatrix} v_1 & v_2 & \dots & v_n \end{bmatrix} \tag{7.3}$$

where v_j is the jth eigenvector of the $\boldsymbol{A}$ matrix and n is the dimension of the $\boldsymbol{A}$ matrix. A new representation is constructed as (Grace *et al.* 1992; Kailath 1980)

$$\frac{\mathrm{d}\tilde{\boldsymbol{x}}}{\mathrm{d}t} = \boldsymbol{P}^{-1}\boldsymbol{A}\boldsymbol{P}\tilde{\boldsymbol{x}} + \boldsymbol{P}^{-1}\boldsymbol{B}u, \tag{7.4}$$

$$z = \boldsymbol{C}\boldsymbol{P}\tilde{\boldsymbol{x}} \tag{7.5}$$

where $\tilde{x} \triangleq \boldsymbol{P}^{-1}x$. The new representation is written as

$$\frac{\mathrm{d}\tilde{\boldsymbol{x}}}{\mathrm{d}t} = \tilde{\boldsymbol{A}}\tilde{x} + \tilde{\boldsymbol{B}}u, \tag{7.6}$$

$$z = \tilde{\boldsymbol{C}}\tilde{\boldsymbol{x}} \tag{7.7}$$

where the real eigenvalues of the original $\boldsymbol{A}$ matrix appear on the diagonal of $\tilde{\boldsymbol{A}}$ and the complex eigenvalues appear in a 2×2 block on the diagonal of $\tilde{\boldsymbol{A}}$. For an $\boldsymbol{A}$

matrix with eigenvalues $(\alpha_1, \sigma \pm j\omega, \alpha_2)$, the $\tilde{\boldsymbol{A}}$ matrix is

$$\tilde{\boldsymbol{A}} = \begin{bmatrix} \alpha_1 & 0 & 0 & 0 \\ 0 & \sigma & \omega & 0 \\ 0 & -\omega & \sigma & 0 \\ 0 & 0 & 0 & \alpha_2 \end{bmatrix}. \tag{7.8}$$

In this form, each state-variable pair represents a mode of the system. Furthermore, the modes are block decoupled so that each mode is represented by the 2×2 system

$$\begin{bmatrix} \dfrac{\mathrm{d}\tilde{x}_1}{\mathrm{d}t} \\ \dfrac{\mathrm{d}\tilde{x}_2}{\mathrm{d}t} \end{bmatrix} = \begin{bmatrix} \sigma & \omega \\ -\omega & \sigma \end{bmatrix} \begin{bmatrix} \tilde{x}_1 \\ \tilde{x}_2 \end{bmatrix} + \begin{bmatrix} \tilde{b}_1 \\ \tilde{b}_2 \end{bmatrix} u, \tag{7.9}$$

$$z_1 = \begin{bmatrix} \tilde{c}_1 & \tilde{c}_2 \end{bmatrix} \begin{bmatrix} \tilde{x}_1 \\ \tilde{x}_2 \end{bmatrix}, \tag{7.10}$$

where ω, σ, $\tilde{b}_1$, $\tilde{b}_2$, $\tilde{c}_1$, and $\tilde{c}_2$ are all scalars. This is known as the modal canonical state-space form. All modes can be monitored directly for high-transient reinforcement in this form.

7.2. *Modal observability and controllability*

It is easy to see that if $\tilde{b}_1$ and $\tilde{b}_2$ are zero, no input can affect the mode and the mode is uncontrollable. Similarly, if $\tilde{c}_1$ and $\tilde{c}_2$ are zero, then the motion of $\tilde{x}_1$ and $\tilde{x}_2$ cannot be measured at the output, z_1, and the mode is unobservable. In terms of stabilization, an uncontrollable mode is not problematic as long as it is stable. However, if an unstable mode is uncontrollable, nothing can be done to stabilize it. Observability may be a problem even if modes are stable. If an unobservable mode is highly amplified by control energy, no attempt could be made to suppress it since it would not be observed at the output. In terms of poles and zeros, uncontrollable or unobservable modes both show up as pole/zero cancellations in the complex s-plane. As can be seen from figure 2, many poles and zeros for the channel system lie on top of each other, indicating that certain modes in the system are either uncontrollable, unobservable, or both. Although a mode may not be physically observable at the output, the modal canonical formulation allows us to numerically observe the state evolution of each mode directly. In this way, we may assess the risk of highly amplified modes triggering bypass transition. This is done for the controlled system simulated in figure 8. The uncontrolled linear system is simulated with an initial condition for 200 time steps at which time a feedback controller with gain $K = 0.1$ is turned on. Figure 11 shows the state evolution of the modes with poles at $s = -0.1474 \pm 0.8514\mathrm{i}$ and $s = -0.3252 \pm 0.6361\mathrm{i}$ as well as the state evolution of the one unstable mode.† In addition, figure 11(*a*) shows the shear measurement at the output. We see that the unstable mode dies out quickly as soon as the feedback is turned on. In addition, the mode at $s = -0.1474 \pm 0.8514\mathrm{i}$ gains almost no energy after the feedback is activated. This indicates that the mode is not a bypass mode. The mode at $s = -0.3252 \pm 0.6361\mathrm{i}$ is seen to gain a lot of energy after the controller is started. Indeed, the amplitude of the transient response is nearly twice that of the unstable mode. This represents a possible bypass mode since such an amplitude

† Note that amplitudes shown as a result of linear system simulations should only be used for comparison with each other since the linear model has been scaled to unity open-loop feedforward gain, i.e. $H(s) = \kappa Z(s)/U(s)$ where $\kappa = 1$.

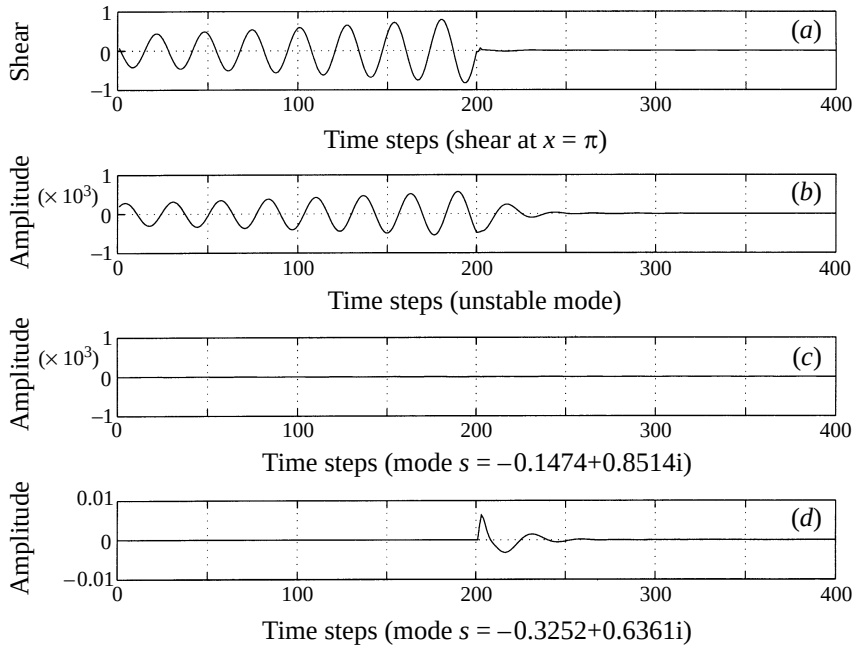

FIGURE 11. Linear model state evolution of system modes with control applied at $t = 200$: (*a*) measured shear, (*b*) the state evolution of the unstable mode, (*c*) the state evolution of the mode at $s = -0.1474 + 0.8514\text{i}$, (*d*) the state evolution of the mode at $s = -0.3252 + 0.6361\text{i}$. Channel model: $Re = 10\,000$, shear sensor at π, $w(x) = \sin(x)$, $L = 4\pi$, $\alpha = 1.0$.

may force the system into the nonlinear region where transition to turbulence may be triggered. Furthermore, the high energy nature of the mode cannot be observed at the shear sensor since this mode is unobservable. This can be seen from the plot of the shear sensor output. Modal un-observability is also suggested by noting the relatively low $\tilde{c}_1$ and $\tilde{c}_2$ values of 0.5155, −0.1131 compared to the $\tilde{c}_1$ and $\tilde{c}_2$ values of −162.85, 234.66 for the unstable mode which is clearly seen at the output. Fortunately, the high energy nature of the mode does not lead to a bypass transition in this case. This is verified by the Navier–Stokes simulation in figure 8, which shows no nonlinear effects. If the instability were allowed to grow to a higher amplitude before the controller was applied, however, the highly amplified mode in the transient response might have triggered nonlinear effects.

8. Multiple instability control

Although most work has focused on suppression of single instabilities, more realistic models should include multiple wavenumbers. Indeed, for a given Reynolds number, an infinite number of wavenumbers exist. Each wavenumber contributes its own poles and zeros to the control-theoretic model. Consider a model with non-dimensional channel length 20π, where input is applied as $w(x) = \sin(x) + \sin(0.9x)$. In this model, wavenumbers of 0.9 and 1.0 are included. Both wavenumbers lead to unstable modes. The pole/zero configuration of this new two-wavenumber model with shear sensor at π is shown in figure 12(*a*). Note that in comparison to the one-wavenumber model, more poles and zeros exist. The original one-wavenumber model contained one 'fork' structure of poles, while the two-wavenumber model contains two 'fork'

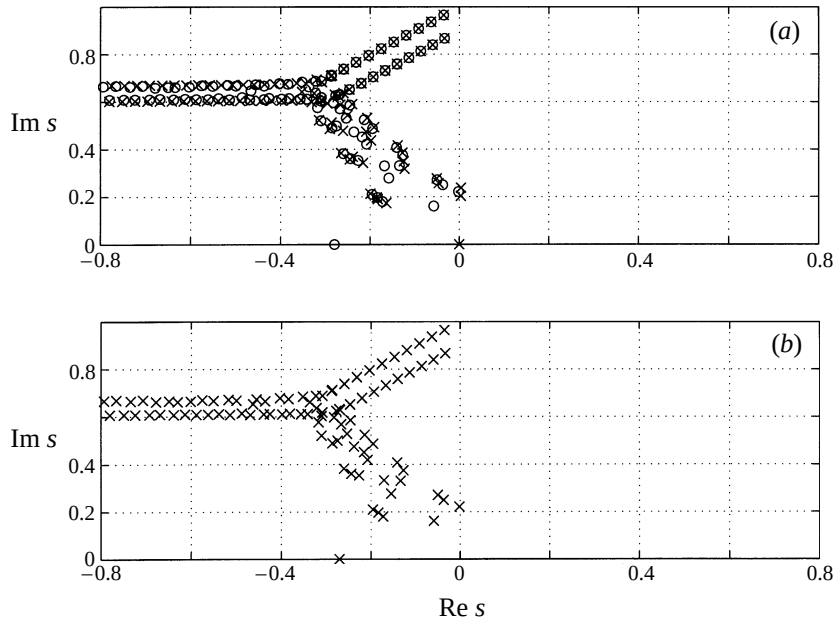

FIGURE 12. (*a*) Pole (×) and zero (o) configuration of channel system of length 20π, including wavenumbers of 0.90 and 1.00. $Re = 10\,000$, shear sensor at π, $w(x) = \sin(x) + \sin(0.9x)$. Only the top half of the *s*-plane is shown. (*b*) Same as (*a*) but showing closed-loop poles after feedback with gain $K = 0.1$.

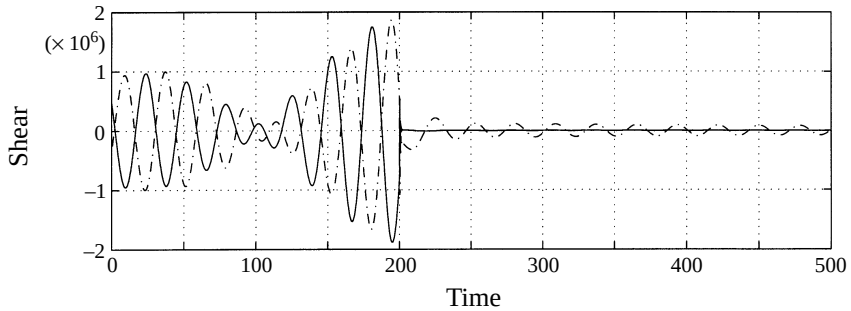

FIGURE 13. Navier–Stokes simulation of channel system of length 20π, including wavenumbers of 0.90 and 1.00. $Re = 10\,000$, feedback shear sensor at π, $w(x) = \sin(x) + \sin(0.9x)$, feedback gain $K = 0.1$. Curve 1 (solid) shows shear at location π; curve 2 (dash-dot) shows shear at location 2π.

structures. It can be visualized that in a model with several wavenumbers, several 'forks' will stack on top of each other in the *s*-plane. Near $s = i0.2$ are two unstable poles in the right-hand plane that represent the two unstable modes in the system. As seen before, all zeros lie in the left hand *s*-plane. Figure 12(*b*) shows the closed-loop poles after feedback with gain $K = 0.1$. Results from the Navier–Stokes simulation are shown in figure 13. The computation is carried out without feedback until $t = 200$. A combination of two growing waves is seen at the shear sensor. At $t = 200$, feedback with integral compensation is applied and the system is stabilized.

9. Effect of linear controllers on two-dimensional finite-amplitude disturbances

The critical Reynolds number above which linear instabilities exist in plane Poiseuille flow is $Re \approx 5772$. Below this Reynolds number, Poiseuille flow is linearly stable. However, transition from laminar to turbulent flow occurs in experiments at much lower Reynolds numbers, typically around $Re = 1000$. Moreover, even for super-critical Reynolds number flows, linear instabilities predict extremely slow growth rates. In practice, transition occurs orders of magnitude more quickly. Therefore, linear stability alone does not dictate transition. Transition to turbulence is generally accepted to be a nonlinear three-dimensional phenomenon. In previous sections, we constructed two-dimensional linear controllers based on the two-dimensional linearized Navier–Stokes equations. By applying these controllers to plane Poiseuille flow with infinitesimal two-dimensional disturbances, we saw that we may linearly stabilize the system so that the flow could no longer support those disturbances. If we apply our linear controllers to flows that contain finite-amplitude disturbances, we can no longer use linear analysis to describe the flow dynamics as nonlinear terms become relevant. However, the application of a controller based on linear analysis does change the nonlinear system.

Many authors (Orszag & Patera 1983; Bayly, Orszag & Herbert 1988) have explored the effect of two-dimensional finite-amplitude disturbances on three-dimensional infinitesimal disturbances in plane Poiseuille flow. Above $Re \approx 2900$, for two dimensions, stable non-attenuating finite-amplitude equilibria exist in plane Poiseuille flow. Below $Re \approx 2900$, non-decaying, finite-amplitude equilibria do not exist. However, in flows with $1000 \leqslant Re \leqslant 2900$, the timescale for decay is so large that the flow may be considered in 'quasi-equilibrium'. It has been shown that in the presence of such two-dimensional finite-amplitude disturbances, infinitesimal three-dimensional disturbances are highly unstable and may cause transition in shear flows. Figure 14 shows the energy of a single-wavenumber, two-dimensional finite-amplitude disturbance ($\alpha = 1.0$) and a single-wavenumber-pair, three-dimensional infinitesimal disturbance ($\alpha = 1.0, \beta = \mp 1.0$) obtained through direct numerical simulation at $Re = 3000$. The maximum amplitude of the two-dimensional finite-amplitude disturbance is $0.1U_c$. At this Reynolds number, wavenumber, and initial energy level, we see the two-dimensional finite-amplitude disturbance decaying slowly. The three-dimensional disturbance, on the other hand, is seen to rapidly gain energy. Orszag & Patera (1983) show that the two-dimensional instability acts as a mediator for transfer of energy from the mean flow to the three-dimensional disturbance, but does not directly provide energy. The growth rate of the three-dimensional disturbance is orders of magnitude larger than that of the Orr–Sommerfeld instabilities.

Orszag & Patera show, in the case where $Re \leqslant 1000$, that the attenuation of finite-amplitude two-dimensional disturbances is large enough that three-dimensional disturbances do not become unstable. The fact that high attenuation of the two-dimensional finite-amplitude disturbance prevented three-dimensional instability below $Re \approx 1000$ suggests that if controllers can be created that speed up the attenuation of the finite-amplitude two-dimensional disturbance for flows with Reynolds numbers greater than 1000, three-dimensional instability may be eliminated. We have seen in §6 that linear controllers did stabilize infinitesimal two-dimensional disturbances. Figure 15 shows the effects of the linear controller of §6 when applied to a system with the same finite-amplitude two-dimensional disturbance and infinitesimal three-dimensional disturbance shown in figure 14. The linear controller

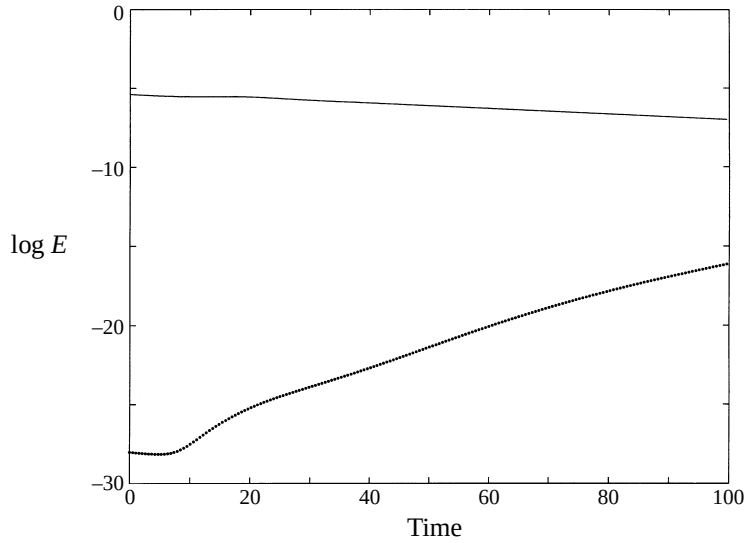

FIGURE 14. Energy of a two-dimensional finite-amplitude disturbance ($\alpha = 1.0$) and a three-dimensional infinitesimal disturbance ($\alpha = 1.0, \beta = \mp 1.0$) for $Re = 3000$. Solid line represents the total energy of the two-dimensional finite-amplitude disturbance and the dotted line represents that of the three-dimensional infinitesimal disturbance.

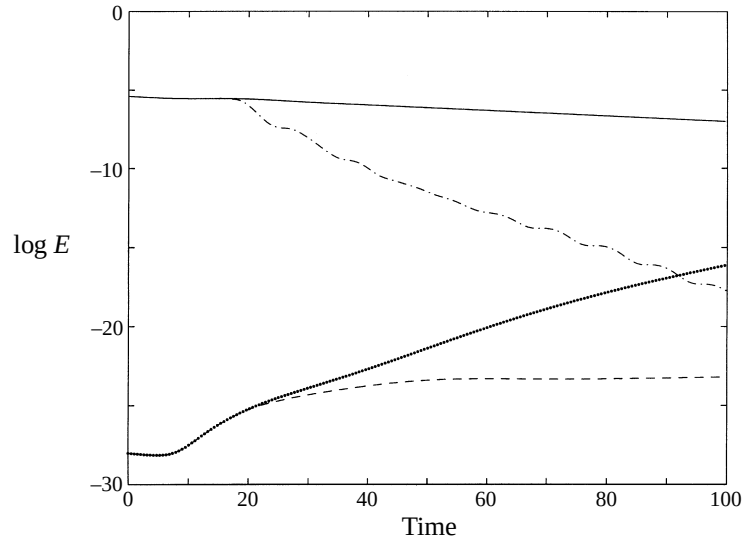

FIGURE 15. Effect of linear controller when applied at $t = 15$ for $Re = 3000$. The top two lines show the two-dimensional finite-amplitude disturbance without (solid) and with (dash-dot) linear control. We see at $t = 15$ that the controlled two-dimensional finite-amplitude disturbance is highly damped. The bottom two lines show the infinitesimal three-dimensional disturbance without (dot) and with (dashed) linear control. That without controller gains energy quickly, while that with controller quickly fails to gain energy.

dramatically increased the attenuation of the finite-amplitude two-dimensional disturbance. As a result, the infinitesimal three-dimensional disturbance was rendered stable. Clearly, the linear controller not only stabilized the two-dimensional linear system, but also had a stabilizing effect on the three-dimensional nonlinear system. These results show the promise of linear controllers even in nonlinear systems.

10. Conclusions

In this paper, we have developed feedback controllers that linearly stabilize plane Poiseuille flow. We used a Galerkin spectral method to generate state-space models. Indeed, any (convergent) numerical method that reduces the governing partial differential equations into a set of ordinary-differential equations may be used. It is important to note, however, that the meaning of the state variables in the state-space model changes as different numerical methods are employed. Even though state variables may not have any specific physical meaning, some numerical methods may result in favourable divisions of system dynamics. In the plane Poiseuille flow case, the spectral Galerkin method with the use of Fourier components in the x-direction and combination-Chebyshev polynomials in the y-direction led to modelled dynamics that were de-coupled by wavenumber. This led to a block diagonal form of the $\boldsymbol{A}$ matrix. As a result, we were clearly able to describe modelled and unmodelled dynamics in terms of wavenumber dynamics included and not included in our finite-dimensional model. This also led us to the concept of using distributed control to render certain wavenumbers 'uncontrollable'. If other numerical methods had been used, this concept would not have been so transparent. Furthermore, plane Poiseuille flow can be linearly stabilized with simple feedback controllers if sensors are placed at judicious locations. Both the position and the type of sensing and actuation change the zeros of single-input/single-output models. In our case, we have seen that certain shear sensor locations lead to 'minimum-phase' systems and some locations lead to 'non-minimum phase' systems. Minimum-phase systems are in general easier to control than non-minimum phase systems. As a result, we were able to stabilize plane Poiseuille flow with a constant gain feedback, integral compensator controller. In addition, the controller was extremely robust to a wide range of Reynolds numbers. Also, we have shown that one danger of feedback control is that the linear transient response of a controlled system can lead to high amplitudes for a short period of time. If these amplitudes are high enough, it is possible that they may invalidate the linear model and enhance nonlinear effects. Furthermore, the high transients may not be observable at the output so that feedback control cannot be used to suppress them. Finally, we have shown that linear controllers have a strong stabilizing effect on two-dimensional finite-amplitude disturbances. As a result, three-dimensional secondary instabilities can be rendered stable.

This research was performed under grant number F49620-93-1-0332 from the United States Air Force. The authors would like to thank Professors J. S. Gibson and Robert Kelly of the UCLA Mechanical and Aerospace engineering department for many helpful discussions and suggestions. The authors are also grateful to Mr. Jaisig Choi who performed the computations presented in §9. Computer resources have been provided by the NAS program at NASA Ames Research Center.

REFERENCES

Bayly, B. J., Orszag, S. A. & Herbert, T. 1988 Instability mechanisms in shear-flow transition. *Ann. Rev. Fluid Mech.* **20**, 359–391.

Beringen, S. 1984 Active control of transition by periodic suction and blowing. *Phys. Fluids* **27**, 1345–1348.

Bower, W. W., Kegelman, J. T. & Pal, A. 1987 A numerical study of two-dimensional instability-wave control based on the Orr-Sommerfeld equation. *Phys. Fluids* **30**, 998–1004.

Bryson, A. E. Jr. & Ho, T.-C. 1975 *Applied Optimal Control*. Taylor and Francis.

Burns, J. A. & Ou Y.-R. 1994 Feedback control of the driven cavity problem using LQR designs. *Proc. 33rd Conf. on Decision and Control, December, 1994*, pp. 289–294.

Butler, K. M. & Farrell, B. F. 1992 Three-dimensional optimal perturbations in viscous shear flows. *Phys. Fluids* A **4**, 1637–1650.

Choi, H., Moin, P. & Kim, J. 1994 Active turbulence control for drag reduction in wall bounded flows. *J. Fluid Mech.* **262**, 75–110.

Drazin, P. G. & Reid, W. H. 1981 *Hydrodynamic Stability*. Cambridge University Press.

Farrell, B. F. 1988 Optimal perturbations in viscous shear flows. *Phys. Fluids* **31**, 2093–2102.

Franklin, G., Powell, J. D. & Emami-Naeini,A. 1988 *Feedback Control of Dynamic Systems*. Addison-Wesley.

Grace, A., Laub, A. J., Little, J. N. & Thompson, C. M. 1992 *Control System Toolbox: For use with MATLAB*. The Math Works.

Gunzburger, M. D., Hou, L. & Svobodny, T. 1992 Boundary velocity control of incompressible flow with an application to viscous drag reduction. *SIAM J. Control Optimization* **30**, 167–181.

Henningson, D. S. 1994 Bypass transition – Proceedings from a Mini-workshop. *Tech. Rep*. Royal Institute of Technology, Department of Mechanics, S-100,44, Stockholm, Sweden.

Joshi, S. S. 1996 A systems theory approach to the control of plane Poiseuille flow. PhD thesis, UCLA, Department of Electrical Engineering,

Joslin, R. D., Erlebacher, G. & Hussaini, M. Y. 1994 Active control of instabilities in laminar boundary layer flow- Part I: An overview. *ICASE Rep*. 94–97. NASA Langley Research Center, Hampton, VA.

Kailath, T. 1980 *Linear Systems*. Prentice-Hall.

Kim, J., Moin, P. & Moser, R. 1987 Turbulence statistics in fully developed channel flow at low Reynolds numbers. *J. Fluid Mech.* **177**, 133–166.

Kreiss, H.-O. & Lorenz, J. 1989 *Initial Boundary Value Problems and the Navier-Stokes Equations*. Academic.

Ladyzhenskaya, O. A. 1969 *The Mathematical Theory of Viscous Incompressible Flow*. Gordon and Breach.

Nosenchuck, D. M. 1982 Passive and active control of boundary layer transition. PhD thesis, California Institute of Technology.

Ogata, K. 1990 *Modern Control Engineering*. Prentice-Hall.

Orr, W. M'F. 1907 The stability or instability of the steady motions of a perfect liquid and of a viscous liquid. *Proc. R. Irish Acad.* A **27**, 9–68.

Orszag, S. A. 1971 Accurate solution of the Orr Sommerfeld stability equation. *J. Fluid Mech.* **50**, 689–703.

Orszag, S. A. & Patera, A. T. 1983 Secondary instability of wall-bounded shear flows. *J. Fluid Mech.* **128**, 347–385.

Reed, H. L. & Nayfeh, A. H. 1986 Numerical perturbation technique for stability of flat plate boundary layer with suction. *AIAA J.* **24**,

Schubauer, G. B. & Skramstad, H. K. 1947 Laminar boundary layer oscillations and stability of laminar flow. *J. Aeronaut. Sci.* **14**, 68–78.

Sommerfeld, A. 1908 Ein Beitrag zur hydrodynamicischen Erklaerung der turbulenten Fluessigkeitsbewegungen. *Proc. 4th Intl Congress of Mathematics*, Vol. III, pp. 116-124.

Temam, R. 1984 *Navier-Stokes Equations*. North-Holland.

Trefethen, L. N., Trefethen, A. E., Reddy, S. C. & Driscoll, T. A. 1993 Hydrodynamic stability without eigenvalues. *Science* **261**, 578–584.